Electronic theory for scanning tunneling microscopy spectra in infinite-layer nickelate superconductors

Peayush Choubey [1,2,*] and Ilya M. Eremin [1]

[1] *Institut für Theoretische Physik III, Ruhr-Universität Bochum, D-44801 Bochum, Germany*

[2] *Department of Physics, Indian Institute of Technology (Indian School of Mines), Dhanbad, Jharkhand 826004, India*

(Received 18 August 2021; accepted 4 October 2021; published 15 October 2021)

The recent scanning tunneling microscopy (STM) observation of U-shaped and V-shaped spectra (and their mixture) in superconducting $Nd_{1-x}Sr_xNiO_2$ thin films has been interpreted as the presence of two distinct gap symmetries in this nickelate superconductor [Gu *et al.*, Nat. Commun. **11**, 6027 (2020)]. Here, using a two-band model of nickelates capturing dominant contributions from Ni-$3d_{x^2-y^2}$ and rare-earth (R)-$5d_{3z^2-r^2}$ orbitals, we show that the experimental observation can be simply explained within a pairing scenario characterized by a conventional $d_{x^2-y^2}$-wave gap structure with the lowest harmonic on the Ni band and a $d_{x^2-y^2}$-wave gap with higher harmonics on the R band. We perform realistic simulations of STM spectra employing first-principles Wannier functions to properly account for the tunneling processes and obtain V, U, and mixed spectral line shapes depending on the position of the STM tip within the unit cell. The V- and U-shaped spectra are contributed by Ni and R bands, respectively, and Wannier functions, in essence, provide position-dependent weighting factors, determining the spectral line shape at a given intra-unit-cell position. We propose a phase-sensitive experiment to distinguish between the proposed d-wave gap structure and the time-reversal symmetry-breaking $d + is$ gap which yields very similar intra-unit-cell spectra.

DOI: 10.1103/PhysRevB.104.144504

I. INTRODUCTION

The recent discovery of superconductivity in thin films of Sr-doped infinite-layer nickelates $RNiO_2$ (R = Nd, Pr, La) [1–5] has garnered significant attention from the condensed matter community. Infinite-layer nickelates were originally envisaged as analogs of cuprate high-T_c superconductors, owing to the $3d^9$ character of Ni^+ [6], the same as Cu^{2+} in cuprates. However, subsequent first-principles calculations [7] showed that, unlike cuprates, nickelates are multiband systems with significant c-axis electronic dispersion and moderate Ni-O hybridization. Recent experiments have further highlighted the difference between these two systems. Parent compounds of infinite-layer nickelates do not show any long-range magnetic order [8–10], however, a recent NMR study suggests antiferromagnetic order in $Nd_{0.85}Sr_{0.15}NiO_2$ powdered samples [11]. Further, the parent compounds of superconducting nickelates are bad metals showing a resistivity upturn at low temperatures (∼70 K) [1,2], which has been attributed to Kondo-like physics [12]. Furthermore, Hall effect measurements [1,2,13,14] and x-ray spectroscopy [15] indicate the multiband character of the parent compound.

The superconducting dome in $RNiO_2$ thin films extends into the hole-doping range ∼(0.12–0.25) [13,14], with the maximum transition temperature $T_c \sim 14$ K occurring in the Pr compound [14]. Although there is no substantive information about the nature of the superconducting state yet, a recent scanning tunneling microscopy (STM) study [16] on superconducting $Nd_{1-x}Sr_xNiO_2$ thin films has revealed the presence of (i) a V-shaped spectrum that fits well to a simple d-wave gap function with a maximum gap of 3.9 meV, (ii) a U-shaped spectrum resembling an s-wave gap with amplitude 2.35 meV, and (iii) spectra showing a mixture of both. Due to the substantial surface roughness of the sample, it was not possible to identify the precise location of the STM tip with respect to the surface atoms.

On the theory front, nickelates have been proposed to harbor unconventional superconductivity as electron-phonon coupling turns out to be too small to produce the observed high T_c [17]. Weak-coupling theories of spin-fluctuation-mediated pairing [17–21] as well as strong-coupling theories based on t-J-like models [22–25] employing a multiband model of the normal state, as predicted by a number of first-principles studies (plane DFT [7,15,18,26–30] as well as calculations taking many-body effects into account [31–38]), predict $d_{x^2-y^2}$-wave pairing in a large region of the parameter space. Note that a cupratelike simple $d_{x^2-y^2}$-wave pairing will result in a V-shaped spectrum and, hence, cannot explain the aforementioned STM results [16] on its own.

To the best of our knowledge, there are three existing explanations of the STM results. First, using a K-t-J model, Ref. [25] proposed that as a function of the doping and Kondo coupling K, the superconducting gap evolves from d wave to s wave with an intermediate $d + is$ state, and thus, one may obtain V-shaped, U-shaped, and mixed spectra if the doping and K change substantially over the sample (which is unlikely, as argued in Ref. [16]). In this scenario, it is hard to explain (without invoking extreme fine-tuning) why the mixed gap shows kinks and coherence peaks at almost

*peayush@gmail.com

the same energies (±2.35 and ±3.9 meV, respectively) [16] where V-shaped and U-shaped spectra show coherence peaks. Second, Ref. [39] proposed that a NiO_2-terminated surface will harbor an extended s-wave gap as opposed to the d-wave gap on a Nd-terminated surface, primarily due to different local dopings. In the presence of a step edge, Josephson coupling between the two regions will result in a $d + is$ state near the edge, leading to an evolution from a V-shaped to a U-shaped gap across the edge. One of the issues here is that the two surfaces are likely to have strong hybridization and not just a weak link, which may lead to a uniform gap symmetry across the edges. Finally, using a two-orbital model, Ref. [20] obtained orbital-selective gaps with d-wave character on the Ni-$d_{x^2-y^2}$ orbital and an extended s-wave gap on the axial orbital. Even though the gap has different symmetries in the orbital space, it must reduce to a unique symmetry in the band space and, hence, cannot explain the STM observation as such.

Here, we propose a simple explanation of the observed STM spectra using a two-band model [15] obtained by downfolding DFT results to Ni-$d_{x^2-y^2}$ and R-$d_{3z^2-r^2}$ orbitals. Assuming d-wave pairing, we hypothesize that the superconducting gap follows a cupratelike lowest-harmonic d-wave gap on the Ni-$d_{x^2-y^2}$ band and a nonmonotonic d-wave gap with higher harmonics on the R-$d_{3z^2-r^2}$ band. We compute the continuum local density of states (LDOS) measured by the STM tip at various intra-unit-cell positions, utilizing a first-principles Wannier function-based approach [40–42] and find U-, V-, and mixed-shaped spectra, in agreement with the experiment. Very similar spectral line shapes are also obtained for the $d + is$ state and we propose a phase-sensitive quasiparticle interference experiment [43] to distinguish between the two.

The paper is organized as follows. In Sec. II, we introduce a mean-field model of superconducting $RNiO_2$ with the aforementioned d-wave gap structure and describe the procedure to compute continuum LDOS at intra-unit-cell points. In Sec. III, we present results detailing intra-unit-cell spectra in nickelates, construct a phase-senstive quasiparticle interference observable [43] to distinguish between d-wave and $d + is$-wave ground states, discuss the theoretical underpinnings of our numerical findings, and comment on the sensitivity of our results on various parameters. Finally, we summarize our findings in Sec. IV.

II. MODEL

We model the homogeneous superconducting state in nickelates by the following mean-field Hamiltonian:

$$H = H_0 + H_{\rm SC}, \tag{1}$$

$$H_0 = \sum_{\mathbf{k},\mu,\nu,\sigma} \epsilon^{\mu\nu}_{\mathbf{k}} c^\dagger_{\mathbf{k}\mu\sigma} c_{\mathbf{k}\nu\sigma} - \mu_0 \sum_{\mathbf{k},\mu,\sigma} c^\dagger_{\mathbf{k}\mu\sigma} c_{\mathbf{k}\mu\sigma}, \tag{2}$$

$$H_{\rm SC} = \sum_{\mathbf{k},\alpha,\sigma} \Delta_\alpha(\mathbf{k}) c^\dagger_{\mathbf{k}\alpha\uparrow} c^\dagger_{-\mathbf{k}\alpha\downarrow} + \text{H.c.} \tag{3}$$

In Eq. (2), $c^\dagger_{\mathbf{k}\mu\sigma}$ creates an electron in the Wannier orbital μ with spin σ and momentum $\mathbf{k}$, $\epsilon^{\mu\nu}_{\mathbf{k}}$ is the normal-state dispersion in the orbital basis, and μ_0 is the chemical potential.

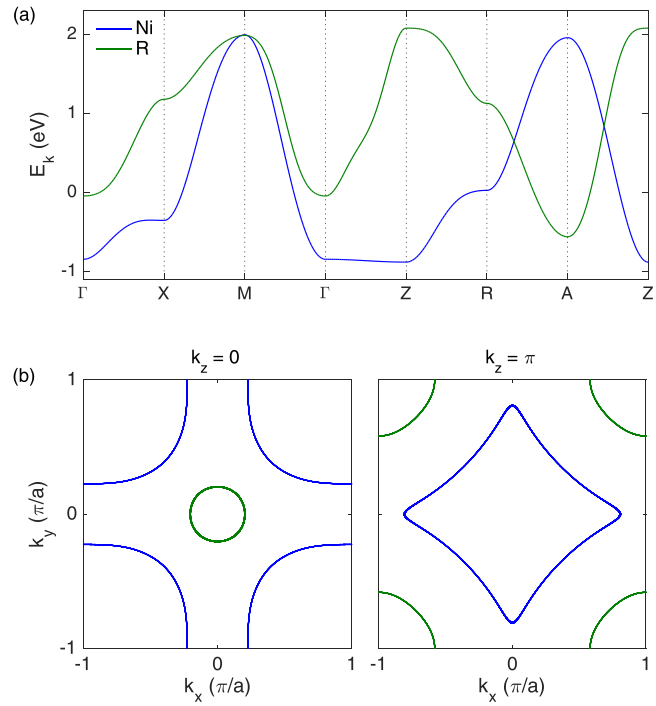

FIG. 1. Characteristic features of the two-band model proposed in Ref. [15]. (a) Band structure of undoped $RNiO_2$ (R = La) along the Γ-Z direction. Blue and green bands have a dominant Ni-$d_{x^2-y^2}$ and R-$d_{3z^2-r^2}$ character, respectively. (b) $k_z = 0$ and (c) $k_z = \pi$ cut of the Fermi surface of 15% hole-doped $RNiO_2$, color coded according to the largest orbital weight. Here, we have set the c-axis lattice constant $c = 1$.

In Eq. (3), $c^\dagger_{\mathbf{k}\alpha\sigma}$ creates an electron in band α with spin σ and momentum $\mathbf{k}$, and $\Delta_\alpha(\mathbf{k})$ is the singlet superconducting gap on band α. To describe the normal state of infinite-layer nickelates, we adopt a two-orbital model for $RNiO_2$ (R = La) obtained by downfolding DFT-derived bands to Ni- and R-centered Wannier orbitals with $d_{x^2-y^2}$ and $d_{3z^2-r^2}$ symmetry, respectively [15]. The R-$d_{3z^2-r^2}$ derived band exhibits a three-dimensional (3D) dispersion, whereas the Ni-$d_{x^2-y^2}$ derived band exhibits a quasi-2D character, similar to that of cuprates, as is evident from the band structure shown in Fig. 1(a). The Ni-$d_{x^2-y^2}$ band contributes to a large holelike Fermi surface, whereas the R-$d_{3z^2-r^2}$ band results in a Fermi surface that changes from a Γ-centered, small electron pocket in the $k_z = 0$ plane to an A-centered electron pocket in the $k_z = \pi$ plane; see Figs. 1(b) and 1(c). We note that the mixing between Ni-$d_{x^2-y^2}$ and R-$d_{3z^2-r^2}$ orbital states is very small for a large energy window leading to the bands with essentially single-orbital characteristics [15]. Ni-$d_{x^2-y^2}$ and R-$d_{3z^2-r^2}$ Wannier orbital's isosurfaces and 2D cuts obtained just above the Ni and R plane are shown in Fig. 2. The Ni-$d_{x^2-y^2}$ Wannier orbital shows more localized and planar characteristics, whereas the R-$d_{3z^2-r^2}$ Wannier orbital is more extended and 3D in nature. Further, the Ni-$d_{x^2-y^2}$ orbital has vanishing weight above the Ni site ($\mathbf{r}_{\rm Ni} = [0, 0, 0]$) as well as along the R-Ni directions due to the $d_{x^2-y^2}$ symmetry, in contrast to the R-$d_{3z^2-r^2}$ orbital, which has a large weight above the R site ($\mathbf{r}_{\rm R} = [0.5a, 0.5a, 0.5c]$, where a and c are lattice constants).

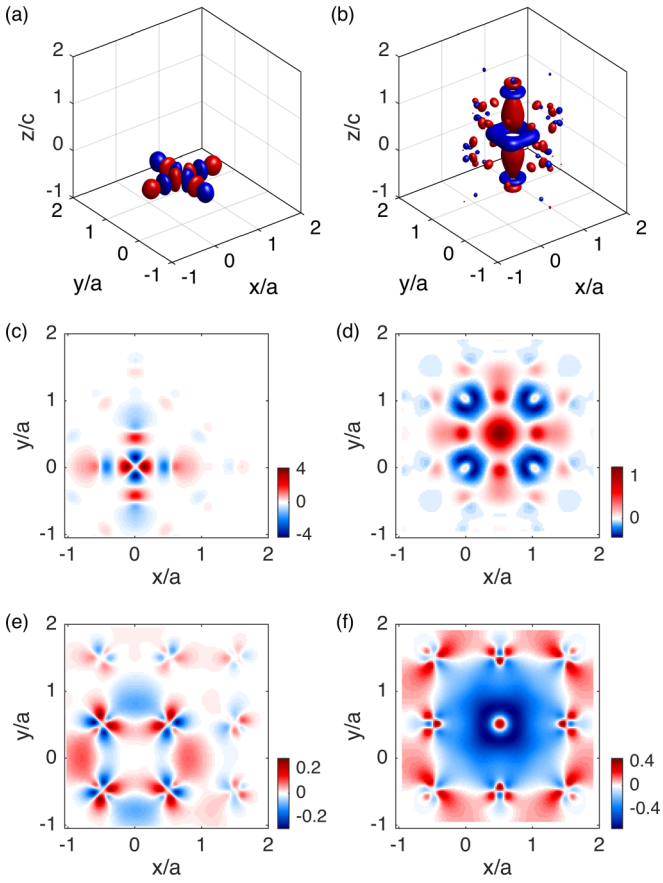

FIG. 2. Ni-$d_{x^2\text{-}y^2}$ and R-$d_{3z^2\text{-}r^2}$ Wannier function isosurfaces and z cuts, taken from Ref. [15]. Isosurface plots of the Ni-$d_{x^2\text{-}y^2}$ (a) and R-$d_{3z^2\text{-}r^2}$ (b) Wannier function at 0.1 Å$^{-3/2}$. Ni-$d_{x^2\text{-}y^2}$ Wannier function at height $z \approx 0.1c$ ($c = 3.89$ Å is the c-axis lattice constant) above the NiO (c) and R (d) planes. R-$d_{3z^2\text{-}r^2}$ Wannier function at height $z \approx 0.1c$ above the NiO (e) and R (f) planes. Color-bar values in (c)–(f) are in units of Å$^{-3/2}$.

Following previous theoretical proposals [17–21], we assume that the superconducting pairing is mostly driven by the Ni-$d_{x^2\text{-}y^2}$ orbital, similarly to hole-doped cuprates, leading to $d_{x^2\text{-}y^2}$-wave gap symmetry. Further, as the Ni-$d_{x^2\text{-}y^2}$ band shows a dispersion very similar to that of the Cu-$d_{x^2\text{-}y^2}$ band in cuprates, it is reasonable to assume that the superconducting gap on the Ni-$d_{x^2\text{-}y^2}$ band can be modeled by a simple lattice version of the $d_{x^2\text{-}y^2}$-wave gap structure as follows:

$$\Delta_{\mathrm{Ni}}(\mathbf{k}) = \frac{\Delta^0_{\mathrm{Ni}}}{2}(\cos k_x - \cos k_y). \tag{4}$$

However, the R-$d_{3z^2\text{-}r^2}$ band shows significant dispersion along k_z, unlike the quasi-2D Ni-$d_{x^2\text{-}y^2}$ band. Although it is still expected that the superconducting gap on this band possesses an overall $d_{x^2\text{-}y^2}$-wave symmetry mostly driven by the the interband Cooper-pair scattering to the dominant quasi-2D Ni-$d_{x^2\text{-}y^2}$ band, it can naturally acquire a significant nonmonotonic behavior on the R-$d_{3z^2\text{-}r^2}$ band. In particular, to explain the aforementioned STM observation [16] and maintain the overall $d_{x^2\text{-}y^2}$-wave symmetry, we propose that the gap on the R-$d_{3z^2\text{-}r^2}$ band has the following form:

$$\Delta_{\mathrm{R}}(\mathbf{k}) = \Delta^0_{\mathrm{R}} \tanh\left[\alpha\left(k_x^2 - k_y^2\right)\right]. \tag{5}$$

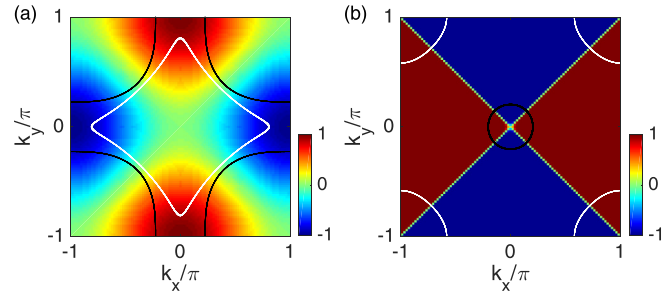

FIG. 3. Single-harmonic and higher-harmonic d-wave gap functions. (a) Conventional, single-harmonic, d-wave gap with the form $\cos(k_x) - \cos(k_y)$, assumed to be present on the Ni-$d_{x^2\text{-}y^2}$ band. (b) Higher-harmonic d-wave gap function with the form $\tanh\alpha(k_x^2 - k_y^2)$ ($\alpha = 100$), assumed to be present on the R-$d_{3z^2\text{-}r^2}$ band. Here, we have set the lattice constant $a = 1$. In both plots, solid black and white lines depict $k_z = 0$ and $k_z = \pi$ Fermi surfaces, respectively, contributed by the respective bands.

Figure 3 shows the gap structure in the k_x-k_y plane along with the $k_z = 0$ and $k_z = \pi$ Fermi surfaces derived from the R-$d_{3z^2\text{-}r^2}$ band. For a sufficiently large value of α, the gap behaves essentially as a step function of the polar angle, sharply changing sign across the nodal directions while maintaining a constant magnitude elsewhere. This nonmonotonic behavior of the superconducting gap is not unusual. For example, the nonmonotonic $d_{x^2\text{-}y^2}$-wave gap is observed in electron-doped cuprates [44,45], which is believed to be due to particular crossing of the AF Brillouin zone boundary with the Fermi surface in these systems. In the superconducting nickelates, the reason for the nonmonotonic dependence of the $d_{x^2\text{-}y^2}$-wave gap on the R-$d_{3z^2\text{-}r^2}$ band could be the more isotropic magnetic response on this band compared to the Ni-$d_{x^2\text{-}y^2}$ band. As we discuss later, this particular gap structure is responsible for the U-shaped partial LDOS contribution from the R band. In addition, we also consider a mixed $d + is$ gap structure [25], where a single-harmonic d-wave gap [Eq. (4)] exists on the Ni band and an s-wave gap with a $\pi/2$ phase difference exists on the R band, i.e., $\Delta_{\mathrm{R}}(\mathbf{k}) = i\Delta^0_{\mathrm{R}}$.

By diagonalizing the normal-state Hamiltonian, Eq. (2), we can obtain the total lattice LDOS $N_{\mathrm{tot}}(\omega) = -\frac{2}{\pi}\mathrm{Im}[\sum_{\mathbf{k}\alpha} G_{\mathbf{k}\alpha}(\omega)]$. Here, the factor of 2 accounts for the spin degeneracy, Im represents the imaginary part, and $G_{\mathbf{k}\alpha}(\omega)$ is the Green's function corresponding to band α, which can be expressed as

$$G_{\mathbf{k}\alpha}(\omega) = \frac{|u_{\mathbf{k}\alpha}|^2}{\omega - E_{\mathbf{k}\alpha} + i0^+} + \frac{|v_{\mathbf{k}\alpha}|^2}{\omega + E_{\mathbf{k}\alpha} + i0^+}, \tag{6}$$

where $|u_{\mathbf{k}\alpha}|^2 = \frac{1}{2}(1 + \frac{\xi_{\mathbf{k}\alpha}}{E_{\mathbf{k}\alpha}})$ and $|v_{\mathbf{k}\alpha}|^2 = \frac{1}{2}(1 - \frac{\xi_{\mathbf{k}\alpha}}{E_{\mathbf{k}\alpha}})$ are the Bogoliubov coherence factors, $E_{\mathbf{k}\alpha} = \sqrt{\xi^2_{\mathbf{k}\alpha} + |\Delta_{\mathbf{k}\alpha}|^2}$ is the quasiparticle energy in the superconducting state, $i0^+$ the artificial broadening, and $\xi_{\mathbf{k}\alpha}$ the band dispersion in the normal state. Moreover, we can obtain the orbital-resolved LDOS $N^{\mu}(\omega) = -\frac{2}{\pi}\mathrm{Im}[\sum_{\mathbf{k}} G^{\mu\mu}_{\mathbf{k}}(\omega)]$ using the orbital-space Green's function $G^{\mu\bar{\mu}}_{\mathbf{k}}(\omega)$, which can be obtained from the band-space Green's function $G_{\mathbf{k}\alpha}(\omega)$ [Eq. (6)] by following the

band-to-orbital basis transformation:

$$G^{\mu\nu}_{\mathbf{k}}(\omega) = \sum_{\alpha} U^{\mu}_{\alpha}(\mathbf{k}) G_{\mathbf{k}\alpha}(\omega) U^{\nu *}_{\alpha}(\mathbf{k}). \tag{7}$$

Here, U^{μ}_{α} are the elements of 2×2 unitary matrix U that diagonalizes the normal-state Hamiltonian $H_0 = \sum_{\mathbf{k}\mu\nu\sigma} c^{\dagger}_{\mathbf{k}\mu\sigma} H^{\mu\nu}_0(\mathbf{k}) c_{\mathbf{k}\nu\sigma}$, with matrix elements $H^{\mu\nu}_0(\mathbf{k}) = \epsilon^{\mu\nu}_{\mathbf{k}} - \mu_0\delta_{\mu\nu}$, yielding the normal-state band dispersion $\xi_{\mathbf{k}\alpha}$.

The differential conductance measured in STM experiments is proportional to the LDOS evaluated at the position of the STM tip [46], and hence, orbital-resolved (or total) lattice LDOS values are not yet the appropriate quantities to compare with experiment, as we need to find LDOS values at continuum positions $\mathbf{r}$ traversed by the STM tip. This can be achieved by a recently developed first-principles Wannier-function-based approach [40–42], which has been applied successfully to interpret and predict various STM observables in cuprates [41,42,47–50] and Fe-based superconductors [40,51,52]. Here, the continuum LDOS at the STM tip position $\mathbf{r}$ is given by $\rho(\mathbf{r},\omega) = -\frac{2}{\pi}\mathrm{Im}[G(\mathbf{r},\omega)]$, where the Green's function $G(\mathbf{r},\omega)$ defined in continuum space is related to the usual lattice Green's function $G^{\mu\nu}_{ij}(\omega)$, which connects orbital μ at site i to orbital ν at site j via a basis transformation, where Wannier functions $W^{\mu}_{i}(\mathbf{r})$ serve as the matrix elements of the transformation:

$$G(\mathbf{r},\omega) = \sum_{ij\mu\nu} W^{\mu}_{i}(\mathbf{r}) G^{\mu\nu}_{ij}(\omega) W^{\nu *}_{j}(\mathbf{r}). \tag{8}$$

Taking the Fourier transform to $\mathbf{k}$ space and using Eq. (7), we obtain

$$G(\mathbf{r},\omega) = \sum_{\mathbf{k}\alpha} G_{\mathbf{k}\alpha}(\omega) |W_{\mathbf{k}\alpha}(\mathbf{r})|^2, \tag{9}$$

$$W_{\mathbf{k}\alpha}(\mathbf{r}) = \sum_{\mu} U^{\mu}_{\alpha}(\mathbf{k}) W^{\mu}_{\mathbf{k}}(\mathbf{r}), \tag{10}$$

$$W^{\mu}_{\mathbf{k}}(\mathbf{r}) = \sum_{i} W^{\mu}_{i}(\mathbf{r}) e^{i\mathbf{k}\cdot\mathbf{R}_i}. \tag{11}$$

Finally, using Eqs. (9)–(11), we can obtain the LDOS at any intra-unit-cell point with a spatial resolution that is limited only by the resolution of the Wannier functions. In what follows, we use this approach to compute the LDOS in x-y planes located at heights slightly above Ni and R atoms, obtaining U, V, and mixed spectral line shapes depending on the location in the planes.

III. RESULTS AND DISCUSSION

We start the discussion of our numerical results by showing in Fig. 4(a) the orbital-resolved lattice LDOS (normalized by the LDOS in the normal state) in the two-band model of $RNiO_2$, Eq. (1), with a simple d-wave gap on the Ni band [Eq. (4)] and higher-harmonic d-wave gap on the R band [Eq. (5)]. Here, we have set the higher-harmonic gap parameter $\alpha = 100$, $\Delta^0_{\mathrm{Ni}} = 4$ meV, and $\Delta^0_{\mathrm{R}} = 2.3$ meV to obtain experimentally reported [16] two-gap features at ± 3.9 and ± 2.35 meV. The Ni LDOS shows the usual V-shaped spectrum expected from a simple d-wave gap, whereas the R-LDOS shows a U-shaped spectrum owing to the higher-harmonic gap structure. In fact, with increasing α, the transition between positive and negative values of the superconducting gap on the R band becomes sharper, leading to a decrease in the magnitude of the slope of the R-LDOS at $\omega = 0$, which becomes vanishingly small at sufficiently large values of α (see Appendix A), resulting in an s-wave-like U-shaped gap on the R band. The $d + is$ gap structure yields a very similar orbital-resolved lattice LDOS; see Fig. 4(b). Thus, at the level of the lattice LDOS, we can explain the experimentally observed V- and U-shaped gaps as orbital-resolved gaps at the Ni and R sites, respectively, emerging from either the higher-harmonic d-wave or $d + is$ gap structure. However, the occurrence of experimentally observed U-V mixed-shaped spectra remains a puzzle, which can be resolved only when we consider the continuum LDOS.

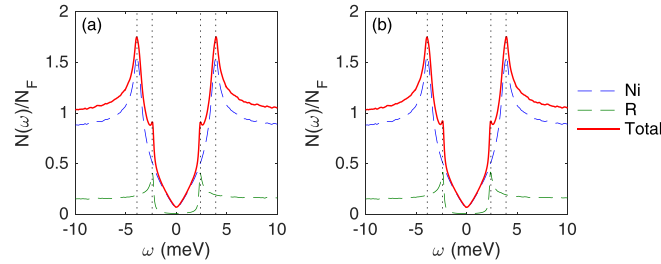

FIG. 4. Lattice density of states spectra. Orbital-resolved lattice LDOS [$N(\omega)$] in the proposed d-wave (a) and $d + is$-wave (b) state, normalized with respect to the Fermi surface DOS (N_F) in the normal state. Dotted vertical lines indicate two sets of coherence peaks, at $\omega = \pm 3.9$ meV and $\omega = \pm 2.35$ meV, contributed by the Ni-$d_{x^2-y^2}$ and R-$d_{3z^2-r^2}$ bands, respectively.

As explained in Sec. II, the correct physical quantity which one should consider when theoretically interpreting STM results is the continuum LDOS evaluated at the STM tip position (and not the lattice LDOS). Figure 5 shows the total continuum LDOS along with contributions from the Ni and R bands at various intra-unit-cell points located in planes right above the Ni and R planes, calculated using Eq. (9) utilizing the Ni-$d_{x^2-y^2}$ and R-$d_{3z^2-r^2}$ Wannier functions [15] described in Sec. II. The LDOS spectra show three distinct line shapes—U shaped, V shaped, and mixed shaped—depending on the position of the intra-unit-cell point. The origin of these distinct line shapes can be understood as follows. Owing to the negligible mixing between the two bands [$U^{\mu}_{\alpha}(\mathbf{k}) \approx \delta_{\alpha\mu}$] for the energies of our interest, the k-space Wannier function in the band space [$W_{\mathbf{k}\alpha}(\mathbf{r})$] [Eq. (11)] and that in the orbital space [$W^{\mu}_{\mathbf{k}}(\mathbf{r})$] are almost identical. Further, the k-space Green's function in the band space is approximately diagonal and equal to the orbital-space Green's function. With these simplifications, the continuum Green's function [Eq. (9)] turns out to be a weighted sum of the k-space Green's function with weighting factors given by k-space Wannier functions: $G(\mathbf{r},\omega) \approx \sum_{\mathbf{k}} G^{\mu\mu}_{\mathbf{k}}(\omega) |W^{\mu}_{\mathbf{k}}(\mathbf{r})|^2$, where $\mu =$ Ni-$d_{x^2-y^2}$ and R-$d_{3z^2-r^2}$. Consequently, we obtain a U (V)-shaped LDOS emerging from the R (Ni) band at the intra-unit-cell points $\mathbf{r}$ where the Ni-$d_{x^2-y^2}$ (R-$d_{3z^2-r^2}$) Wannier function's contribution is negligible. A U-V mixed line shape is obtained at the points where the contributions from both Wannier functions are comparable. Our results are consistent with recent STM experiments [16] and show that the mixture of U- and V-shaped gaps can still

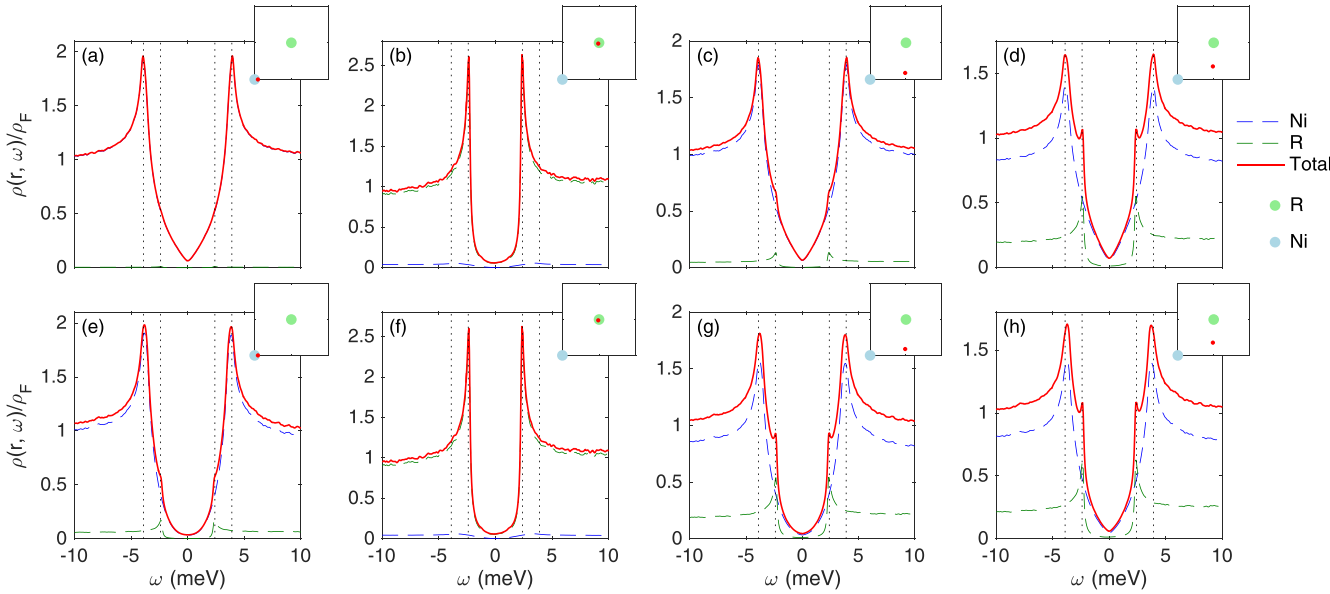

FIG. 5. Distinct spectral line shapes displayed by the continuum LDOS in the higher-harmonic d-wave state. Band-resolved continuum LDOS [$\rho(\mathbf{r}, \omega)$] in the proposed d-wave state (normalized with respect to the Fermi surface LDOS (ρ_F)) at a number of intra-unit-cell points in the x-y plane located at a height $z \approx 0.1c$ above the NiO plane (a)–(d) and R plane (e)–(h). Contributions to the total LDOS (red curves) by Ni and R bands are represented by dashed blue and green lines, respectively. In each panel, the inset shows the position of the intra-unit-cell point (red dot) relative to the Ni (filled light-blue circle) and R (filled light-green circle) positions. Dotted vertical lines indicate two sets of coherence peaks, at $\omega = \pm 3.9$ meV and $\omega = \pm 2.35$ meV.

be a signature of the global d-wave gap. A more detailed STM investigation on a high-quality sample is required to further test our hypothesis. The sample used in Ref. [16] exhibited a large surface roughness (of order 1 nm), making it impossible to ascertain the precise location of the STM tip relative to Ni/R atoms. If such assignments can be made in future experiments, then our theory can be easily tested. Figure 6 shows the spectra obtained along three directions, namely, Ni-R, Ni-O, and R-O, in a plane right above the NiO plane. We find that in the Ni-O direction [Fig. 6(a)], the spectral line shapes change from mixed U-V with both coherence peaks (at ± 2.35 and ± 3.9 meV) to a U-shaped gap with coherence peaks only at the lower gap edge (at ± 2.35 meV). In contrast, the line shapes change from a U-shape (with coherence peaks at the lower gap edge) to a V-shape (with coherence peaks at the higher gap edge) via a mixed U-V shape (with coherence peaks at both gap edges) along the R-O direction [Fig. 6(c)].

The continuum LDOS line shapes at a given intra-unit-cell point are very similar for both the higher-harmonic d-wave gap model and the $d + is$-gap model. Thus, by itself the experimental data [16] cannot rule out the global d-wave gap in infinite-layer nickelates but instead call for further investigations. We recall that the two scenarios can be distinguished by a method proposed by Hirschfeld, Altenfeld, Eremin, and Mazin (HAEM) [43], which is designed to determine the sign structure of the superconducting gap in a multiband system by utilizing the quasiparticle interference information from STM measurements. Followinge HAEM's prescription, we construct the antisymmetrized impurity-induced LDOS $\delta\rho^-(\omega) = \delta\rho(\omega) - \delta\rho(-\omega)$ using the T-matrix formalism; see Appendix B for details. $\delta\rho^-(\omega)$ shows different behavior depending on whether the impurity substitutes the Ni site or the R site. In the former case, it shows identical behavior for both higher-harmonic d-wave and $d + is$-wave gaps, attaining the minimum value near the second gap edge (at 3.9 meV) without any change of sign; see Fig. 7(b). A very similar behavior in the case of single-band cuprates was observed in Ref. [49]. However, in the latter case where an R site is substituted by an impurity, $\delta\rho^-(\omega)$ changes sign and has a much smaller magnitude in the $d + is$ state, whereas it shows a minimum at the lower gap edge (2.35 meV) without any sign change for the higher-harmonic d-wave state; see Fig. 7(a). Therefore, the main difference in the HAEM signal occurs for the impurity at the R site due to the very different phase structure of the gap on the R band in both cases. This is the scenario which can be used to distinguish between the two gap structures.

IV. CONCLUSION

To conclude, we have presented a theoretical analysis of the U-, V-, and mixed-shape spectra observed in a recent STM study on superconducting $Nd_{1-x}Sr_xNiO_2$ thin films assuming a global d-wave symmetry of the superconducting state. Starting with a recently proposed two-orbital model for the normal state of $RNiO_2$ (R = La), which yields a quasi-2D band with Ni-$d_{x^2-y^2}$ character (very similar to that of cuprates) and a 3D band with R-$d_{3z^2-r^2}$ character exhibiting strong dispersion in the Γ-Z direction, we assumed that a global d-wave symmetric superconducting state is driven by the Ni $3d_{x^2-y^2}$ band, resulting in a simple $(\cos k_x - \cos k_y)$ form of the superconducting gap on the same, mirroring hole-doped cuprates. Further, we conjectured that the superconducting

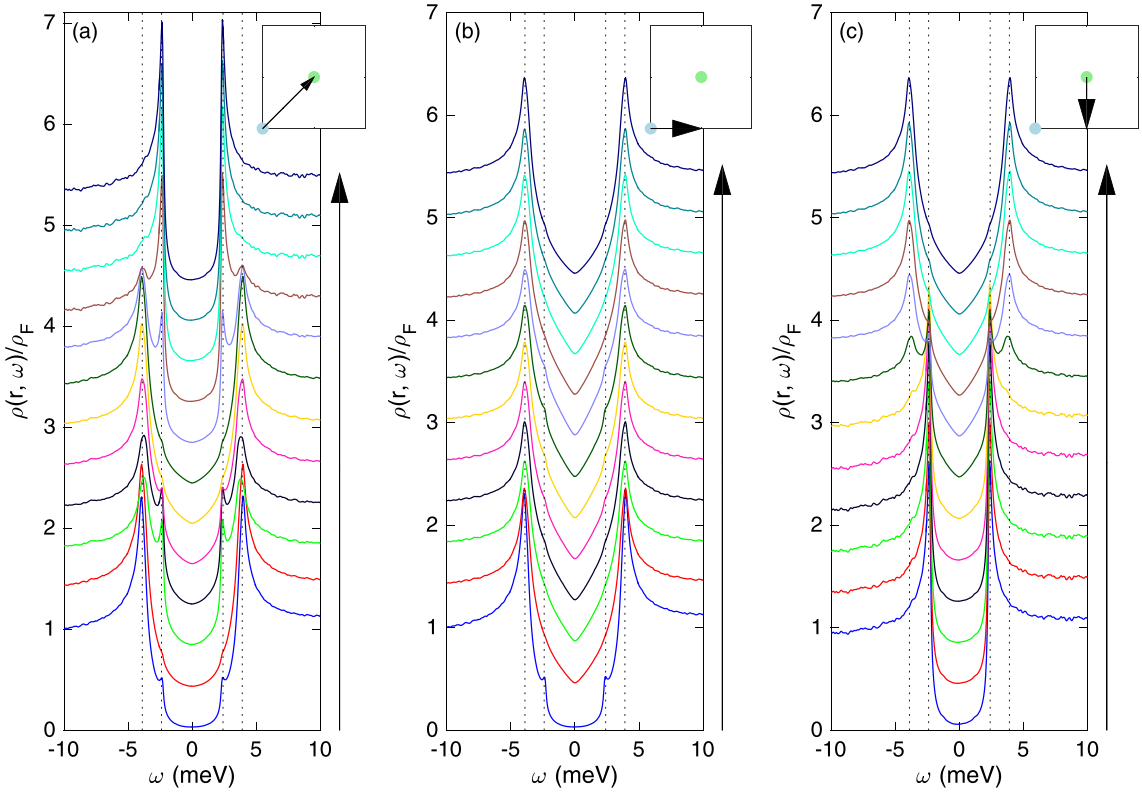

FIG. 6. Spectral line cuts in the higher-harmonic d-wave state along the Ni-R (a), Ni-O (b), and R-O (c) directions in the x-y plane located at a height $z \approx 0.1c$ above the NiO plane. Each spectrum is offset by 0.4 for clarity. Black arrows in insets indicate the cut directions with respect to the Ni (light-blue filled circle) and R (light-green filled circle) positions in the x-y plane. Dotted vertical lines indicate two sets of coherence peaks, at $\omega = \pm 3.9$ meV and $\omega = \pm 2.35$ meV.

gap on the R band consisted of higher d-wave harmonics that can be represented in the $\tanh(\alpha(k_x^2 - k_y^2))$ form. This results in a V-shaped lattice LDOS at the Ni site and, for sufficiently large α, a U-shaped LDOS at the R site. The correct quantity to compare with the differential conductance spectra measured by STM is the continuum LDOS, however, which we computed using first-principles Ni-$d_{x^2\text{-}y^2}$ and R-$d_{3z^2\text{-}r^2}$ Wannier functions reported in Ref. [15]. We found that depending on the intra-unit-cell position, U-, V-, and mixed-shape spectra can be obtained within a $RNiO_2$ unit cell.

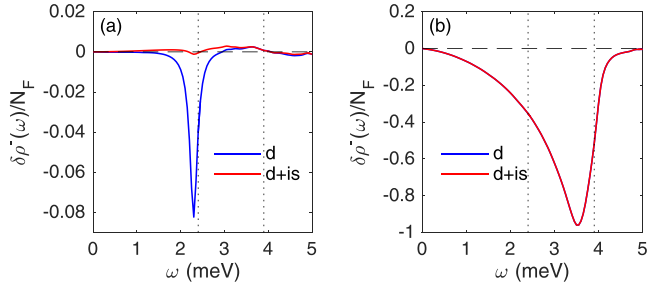

FIG. 7. HAEMS signature of the proposed d-wave and $d + is$-wave states. Antisymmetrized correction to the lattice LDOS due to scattering off a weak pointlike impurity substituting a R atom (a) and a Ni atom (b) in the proposed d-wave state and $d + is$-wave state. Dotted vertical lines indicate positive coherence peaks at $\omega = 3.9$ meV and $\omega = 2.35$ meV.

In essence, the k-space Wannier functions act as weighting factors for Green's functions contributed by the Ni and R bands, yielding a U-shaped (V-shaped) continuum LDOS at the intra-unit-cell positions where contributions from the R-$d_{3z^2\text{-}r^2}$ (Ni-$d_{x^2\text{-}y^2}$) Wannier function dominate. A mixed-shape spectrum is obtained at the positions where both Wannier functions make comparable contributions.

The scenario we proposed can be tested in future STM experiments with improved sample quality where the position of the STM tip with respect to the $RNiO_2$ unit cell can be precisely determined. In particular, line scans along the Ni-R and R-O directions should yield spectral line shapes evolving from mixed to U-shaped and U- to V-shaped, respectively. Further, we showed that a $d + is$-gap structure yields spectra nearly identical to the higher-harmonic d-wave gap model and the two scenarios can be distinguished by phase-sensitive quasiparticle interference measurements on $RNiO_2$ samples with R sites substituted by impurities. Finally, we note that further work is required to understand the genesis of the higher-harmonic d-wave gap from a microscopic theory, which we intend to pursue in future. Typically, multiorbital FLEX calculations of the Cooper-pairing instabilities [18] were done by linearizing the gap equations, which are valid essentially only close to T_c. At the same time, the full temperature and angular evolution of the gap, especially on the passive bands, not actively involved in the Cooper pairing, can only be understood by solving the nonlinear version of the gap equations.

ACKNOWLEDGMENTS

The authors wish to acknowledge useful discussions with F. Lechermann, H. H. Wen, F. Jakubczyk, A. Römer, and B. M. Andersen. The authors are grateful to T. P. Devereaux and Chunjing Jia for providing the Wannier function data published in Ref. [15]. The work was supported by a joint NSFC-DFG grant (No. ER 463/14-1)

APPENDIX A: U-SHAPED LATTICE LDOS IN THE HIGHER-HARMONIC *d*-WAVE STATE

In this Appendix, we show that the higher-harmonic d-wave gap function in Eq. (5) leads to a lattice LDOS that varies linearly with bias at low energies: $N(\omega) = \gamma|\omega|$ for $\omega \to 0$, with slope $\gamma \propto 1/\alpha$, which becomes very small for sufficiently large values of the higher-harmonic gap parameter α, resulting in a U-shaped spectrum. We begin with the spectral function in the superconducting state,

$$A_\sigma(\mathbf{k},\omega) = |u_\mathbf{k}|^2\delta(\omega - E_\mathbf{k}) + |v_\mathbf{k}|^2\delta(\omega + E_\mathbf{k}), \tag{A1}$$

where the coherence factors and quasiparticle energy are given by

$$|u_\mathbf{k}|^2 = \frac{1}{2}\left(1 + \frac{\xi_\mathbf{k}}{E_\mathbf{k}}\right) = 1 - |v_\mathbf{k}|^2, \tag{A2}$$

$$E_\mathbf{k} = \sqrt{\xi_\mathbf{k}^2 + \Delta_\mathbf{k}^2}, \tag{A3}$$

with normal-state dispersion $\xi_\mathbf{k}$ and gap function $\Delta_\mathbf{k}$, which is given by the higher-harmonic d-wave form in Eq. (5). In what follows, we work in units where $\hbar = 1$, suppress the spin index σ, and set the lattice constant $a = 1$ so that the higher-harmonic gap coefficient α can be taken as a dimensionless constant. For $\omega > 0$, the lattice LDOS can be expressed as

$$N(\omega) = 2\sum_\mathbf{k} A(\mathbf{k},\omega) = \int \frac{d\mathbf{k}}{(2\pi)^2}\left(1 + \frac{\xi_\mathbf{k}}{E_\mathbf{k}}\right)\delta(\omega - E_\mathbf{k}). \tag{A4}$$

At low energies, dominant contributions to the integral in Eq. (A4) will be from nodal regions. Accordingly, we can approximate the integral as

$$N(\omega \to 0) \approx M\int_\Omega \frac{d\mathbf{k}}{(2\pi)^2}\left(1 + \frac{\xi_\mathbf{k}}{E_\mathbf{k}}\right)\delta(\omega - E_\mathbf{k}), \tag{A5}$$

where $M = 4$ is the number of nodes and Ω is a small circular region of radius Γ around a nodal point $\mathbf{k}_0$; see Fig. 8. Further, to facilitate the computation of the integral, we introduce a new coordinate system with the origin at $\mathbf{k}_0$ and axes k_1 and k_2 along and perpendicular to the corresponding nodal direction, respectively; see Fig. 8. Furthermore, we expand $\xi_\mathbf{k}$ and $\Delta_\mathbf{k}$ around the node up to linear order. The result can be expressed in the new coordinate system as

$$\xi_\mathbf{k} \approx v_F k_1, \tag{A6}$$

$$\Delta_\mathbf{k} \approx -v_\Delta k_2, \tag{A7}$$

where v_F is the Fermi velocity at the node and

$$v_\Delta = 2\alpha\Delta_0 k_0. \tag{A8}$$

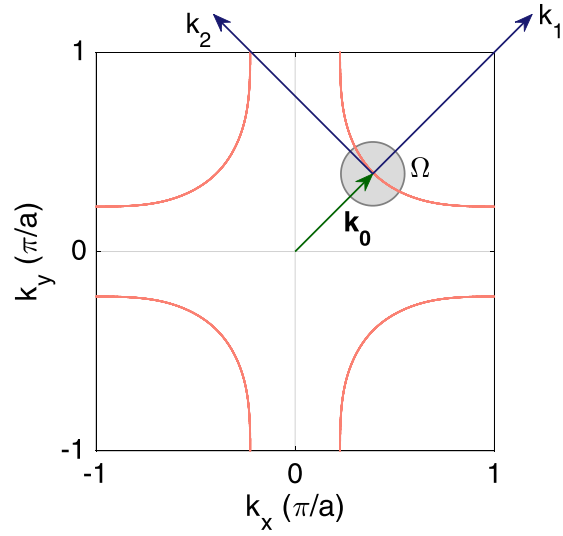

FIG. 8. Schematic of a representative Fermi surface superimposed on a nodal coordinate system with the origin at the nodal point $\mathbf{k}_0$ (green arrow) and axes k_1 and k_2 parallel and perpendicular to the nodal direction, respectively. The region of integration Ω in Eq. (A5) is shown by the filled gray circle around the node.

We note that in the case of the simple d-wave gap, $v_\Delta = \sqrt{2}\Delta_0 \sin(k_0/\sqrt{2})$. Now, first substituting Eqs. (A6) and (A7) into Eq. (A5), then scaling the coordinates, $k_1' = v_F k_1$, $k_2' = v_\Delta k_2$, and finally moving to the polar coordinates, $k_1' = k'\cos\theta'$, $k_2' = k'\sin\theta'$, we obtain

$$N(\omega) = \frac{M}{(2\pi)^2}\frac{1}{v_F v_\Delta}(I_1 + I_2), \tag{A9}$$

$$I_1 = \int_0^{2\pi} d\theta' \int_0^\Gamma k' dk' \delta(\omega - k'), \tag{A10}$$

$$I_2 = \int_0^{2\pi} d\theta' \cos\theta' \int_0^\Gamma k' dk' \delta(\omega - k'). \tag{A11}$$

Clearly, $I_1 = 2\pi\omega$ and $I_2 = 0$, thus the low-energy LDOS for $\omega > 0$ is given by

$$N(\omega) = \left(\frac{M}{2\pi v_F v_\Delta}\right)\omega. \tag{A12}$$

Similarly, we can obtain the LDOS for $\omega < 0$. Combining both, we get

$$N(\omega) = \left(\frac{1}{\pi v_F \Delta_0 k_0 \alpha}\right)|\omega|, \tag{A13}$$

where we have used Eq. (A8) and $M = 4$. Thus, we see that the lattice LDOS at low energies varies linearly with bias with slope $\gamma = 1/(\pi v_F \Delta_0 k_0 \alpha)$, which can be very small at sufficiently large values of α, leading to a U-shaped spectrum.

APPENDIX B: CALCULATION OF THE ANTISYMMETRIZED CORRECTION TO THE LDOS DUE TO IMPURITY SCATTERING

This Appendix provides a detailed description of the T-matrix formalism as applied to the construction of the

antisymmetrized impurity-induced LDOS $\delta\rho^-(\omega) = \delta\rho(\omega) - \delta\rho(-\omega)$ (Fig. 7) used in HAEM's scheme [43]. We begin with the calculation of the local Green's function $\hat{G}_0(\omega) = \sum_{\mathbf{k}} \hat{G}_{\mathbf{k}}(\omega)$, where $\hat{G}$ is the matrix Green's function in the orbital space with elements given by Eq. (7). Now, the T matrix for scattering off a pointlike impurity substituting a lattice site (Ni or R) in the $RNiO_2$ unit cell will be given by

$$\hat{T}(\omega) = [\mathbb{1} - \hat{V}\hat{G}_0(\omega)]^{-1}\hat{V}. \tag{B1}$$

Here, $\mathbb{1}$ represents the identity matrix and $\hat{V} = \tau_3 \otimes \mathrm{diag}([V_{\mathrm{imp}}^{Ni}, V_{\mathrm{imp}}^{R}])$ is the impurity potential in Nambu space, where τ_i is a Pauli matrix, diag represents a diagonal matrix, and $V_{\mathrm{imp}}^{\mathrm{Ni(R)}}$ is the on-site scattering potential for the impurity substituting an Ni (R) site. The impurity-induced change in the local Green's function can be obtained as

$$\delta\hat{G}(\omega) = \hat{G}_0(\omega)\hat{T}(\omega)\hat{G}_0(\omega). \tag{B2}$$

The corresponding (wave-vector-integrated) change in the total LDOS will be given by the following expression [49]:

$$\delta\rho(\omega) = -\frac{1}{\pi}\mathrm{Im}\left[\mathrm{Tr}\frac{(\tau_0 + \tau_3)}{2}\delta\hat{G}(\omega)\right]. \tag{B3}$$

Using Eq. (B3), we can compute the antisymmetrized impurity-induced LDOS $\delta\rho^-(\omega) = \delta\rho(\omega) - \delta\rho(-\omega)$ shown in Fig. 7. Finally, we note that distinction between different gap symmetries on the basis of $\delta\rho^-(\omega)$ occurs in ω space, and therefore, it is sufficient to work at the level of the lattice LDOS; the continuum LDOS should yield the same conclusions as the lattice LDOS, as demonstrated in Ref. [49].

[1] D. Li, K. Lee, B. Y. Wang, M. Osada, S. Crossley, H. R. Lee, Y. Cui, Y. Hikita, and H. Y. Hwang, Superconductivity in an infinite-layer nickelate, Nature (London) **572**, 624 (2019).

[2] M. Osada, B. Y. Wang, B. H. Goodge, K. Lee, H. Yoon, K. Sakuma, D. Li, M. Miura, L. F. Kourkoutis, and H. Y. Hwang, A superconducting praseodymium nickelate with infinite layer structure, Nano Lett. **20**, 5735 (2020).

[3] S. W. Zeng, C. J. Li, L. E. Chow, Y. Cao, Z. T. Zhang, C. S. Tang, X. M. Yin, Z. S. Lim, J. X. Hu, P. Yang, and A. Ariando, Superconductivity in infinite-layer lanthanide nickelates, arXiv:2105.13492.

[4] M. Osada, B. Y. Wang, B. H. Goodge, S. P. Harvey, K. Lee, D. Li, L. F. Kourkoutis, and H. Y. Hwang, Nickelate superconductivity without rare-earth magnetism: (La,Sr)NiO_2, Adv. Mater. 2104083 (2021).

[5] Y. Nomura and R. Arita, Superconductivity in infinite-layer nickelates, arXiv:2107.12923.

[6] V. I. Anisimov, D. Bukhvalov, and T. M. Rice, Electronic structure of possible nickelate analogs to the cuprates, Phys. Rev. B **59**, 7901 (1999).

[7] K.-W. Lee and W. E. Pickett, Infinite-layer $LaNiO_2$: Ni^{1+} is not Cu^{2+}, Phys. Rev. B **70**, 165109 (2004).

[8] A. Ikeda, Y. Krockenberger, H. Irie, M. Naito, and H. Yamamoto, Direct observation of infinite NiO_2 planes in $LaNiO_2$ films, Appl. Phys. Express **9**, 061101 (2016).

[9] M. A. Hayward and M. Rosseinsky, Synthesis of the infinite layer Ni(I) phase $NdNiO_{2+x}$ by low temperature reduction of $NdNiO_3$ with sodium hydride, Solid State Sci. **5**, 839 (2003).

[10] M. A. Hayward, M. A. Green, M. J. Rosseinsky, and J. Sloan, Sodium hydride as a powerful reducing agent for topotactic oxide deintercalation: Synthesis and characterization of the nickel(I) oxide $LaNiO_2$, J. Am. Chem. Soc. **121**, 8843 (1999).

[11] Y. Cui, C. Li, Q. Li, X. Zhu, Z. Hu, Y.-f. Yang, J. Zhang, R. Yu, H.-H. Wen, and W. Yu, NMR evidence of antiferromagnetic spin fluctuations in $Nd_{0.85}$ $Sr_{0.15}$ NiO_2, Chin. Phys. Lett. **38**, 067401 (2021).

[12] G.-M. Zhang, Y.-f. Yang, and F.-C. Zhang, Self-doped Mott insulator for parent compounds of nickelate superconductors, Phys. Rev. B **101**, 020501(R) (2020).

[13] D. Li, B. Y. Wang, K. Lee, S. P. Harvey, M. Osada, B. H. Goodge, L. F. Kourkoutis, and H. Y. Hwang, Superconducting Dome in $Nd_{1-x}Sr_xNiO_2$ Infinite Layer Films, Phys. Rev. Lett. **125**, 027001 (2020).

[14] M. Osada, B. Y. Wang, K. Lee, D. Li, and H. Y. Hwang, Phase diagram of infinite layer praseodymium nickelate $Pr_{1-x}Sr_xNiO_2$ thin films, Phys. Rev. Mater. **4**, 121801(R) (2020).

[15] M. Hepting, D. Li, C. J. Jia, H. Lu, E. Paris, Y. Tseng, X. Feng, M. Osada, E. Been, Y. Hikita, Y.-D. Chuang, Z. Hussain, K. J. Zhou, A. Nag, M. Garcia-Fernandez, M. Rossi, H. Y. Huang, D. J. Huang, Z. X. Shen, T. Schmitt *et al.*, Electronic structure of the parent compound of superconducting infinite-layer nickelates, Nat. Mater. **19**, 381 (2020).

[16] Q. Gu, Y. Li, S. Wan, H. Li, W. Guo, H. Yang, Q. Li, X. Zhu, X. Pan, Y. Nie, and H.-H. Wen, Single particle tunneling spectrum of superconducting $Nd_{1-x}Sr_xNiO_2$ thin films, Nat. Commun. **11**, 6027 (2020).

[17] Y. Nomura, M. Hirayama, T. Tadano, Y. Yoshimoto, K. Nakamura, and R. Arita, Formation of a two-dimensional single-component correlated electron system and band engineering in the nickelate superconductor $NdNiO_2$, Phys. Rev. B **100**, 205138 (2019).

[18] H. Sakakibara, H. Usui, K. Suzuki, T. Kotani, H. Aoki, and K. Kuroki, Model Construction and a Possibility of Cupratelike Pairing in a New d^9 Nickelate Superconductor (Nd, Sr)NiO_2, Phys. Rev. Lett. **125**, 077003 (2020).

[19] X. Wu, D. Di Sante, T. Schwemmer, W. Hanke, H. Y. Hwang, S. Raghu, and R. Thomale, Robust $d_{x^2-y^2}$-wave superconductivity of infinite-layer nickelates, Phys. Rev. B **101**, 060504(R) (2020).

[20] P. Adhikary, S. Bandyopadhyay, T. Das, I. Dasgupta, and T. Saha-Dasgupta, Orbital-selective superconductivity in a two-band model of infinite-layer nickelates, Phys. Rev. B **102**, 100501(R) (2020).

[21] P. Werner and S. Hoshino, Nickelate superconductors: Multiorbital nature and spin freezing, Phys. Rev. B **101**, 041104(R) (2020).

[22] L.-H. Hu and C. Wu, Two-band model for magnetism and superconductivity in nickelates, Phys. Rev. Research **1**, 032046(R) (2019).

[23] Y.-H. Zhang and A. Vishwanath, Type-II *t-J* model in superconducting nickelate $Nd_{1-x}Sr_xNiO_2$, Phys. Rev. Research **2**, 023112 (2020).

[24] M. Kitatani, L. Si, O. Janson, R. Arita, Z. Zhong, and K. Held, Nickelate superconductors—A renaissance of the one-band Hubbard model, npj Quantum Mater. **5**, 59 (2020).

[25] Z. Wang, G.-M. Zhang, Y.-f. Yang, and F.-C. Zhang, Distinct pairing symmetries of superconductivity in infinite-layer nickelates, Phys. Rev. B **102**, 220501(R) (2020).

[26] A. S. Botana and M. R. Norman, Similarities and Differences between $LaNiO_2$ and $CaCuO_2$ and Implications for Superconductivity, Phys. Rev. X **10**, 011024 (2020).

[27] J. Gao, S. Peng, Z. Wang, C. Fang, and H. Weng, Electronic structures and topological properties in nickelates $Ln_{n+1}Ni_nO_{2n+2}$, Natl. Sci. Rev. **8**, nwaa218 (2021).

[28] P. Jiang, L. Si, Z. Liao, and Z. Zhong, Electronic structure of rare-earth infinite-layer $RNiO_2$(R = La, Nd), Phys. Rev. B **100**, 201106(R) (2019).

[29] E. Been, W.-S. Lee, H. Y. Hwang, Y. Cui, J. Zaanen, T. Devereaux, B. Moritz, and C. Jia, Electronic Structure Trends Across the Rare-Earth Series in Superconducting Infinite-Layer Nickelates, Phys. Rev. X **11**, 011050 (2021).

[30] F. Bernardini, V. Olevano, and A. Cano, Magnetic penetration depth and T_c in superconducting nickelates, Phys. Rev. Research **2**, 013219 (2020).

[31] F. Lechermann, Late transition metal oxides with infinite-layer structure: Nickelates versus cuprates, Phys. Rev. B **101**, 081110(R) (2020).

[32] F. Lechermann, Multiorbital Processes Rule the $Nd_{1-x}Sr_xNiO_2$ Normal State, Phys. Rev. X **10**, 041002 (2020).

[33] Y. Wang, C.-J. Kang, H. Miao, and G. Kotliar, Hund's metal physics: From $SrNiO_2$ to $LaNiO_2$, Phys. Rev. B **102**, 161118(R) (2020).

[34] V. Olevano, F. Bernardini, X. Blase, and A. Cano, Ab initio many-body GW correlations in the electronic structure of $LaNiO_2$, Phys. Rev. B **101**, 161102(R) (2020).

[35] F. Petocchi, V. Christiansson, F. Nilsson, F. Aryasetiawan, and P. Werner, Normal State of $Nd_{1-x}Sr_xNiO_2$ from Self-Consistent GW + EDMFT, Phys. Rev. X **10**, 041047 (2020).

[36] S. Ryee, H. Yoon, T. J. Kim, M. Y. Jeong, and M. J. Han, Induced magnetic two-dimensionality by hole doping in the superconducting infinite-layer nickelate $Nd_{1-x}Sr_xNiO_2$, Phys. Rev. B **101**, 064513 (2020).

[37] J. Karp, A. S. Botana, M. R. Norman, H. Park, M. Zingl, and A. Millis, Many-Body Electronic Structure of $NdNiO_2$ and $CaCuO_2$, Phys. Rev. X **10**, 021061 (2020).

[38] I. Leonov, S. L. Skornyakov, and S. Y. Savrasov, Lifshitz transition and frustration of magnetic moments in infinite-layer $NdNiO_2$ upon hole doping, Phys. Rev. B **101**, 241108(R) (2020).

[39] X. Wu, K. Jiang, D. D. Sante, W. Hanke, A. P. Schnyder, J. Hu, and R. Thomale, Surface s-wave superconductivity for oxide-terminated infinite-layer nickelates, arXiv:2008.06009.

[40] P. Choubey, T. Berlijn, A. Kreisel, C. Cao, and P. J. Hirschfeld, Visualization of atomic-scale phenomena in superconductors: Application to FeSe, Phys. Rev. B **90**, 134520 (2014).

[41] A. Kreisel, P. Choubey, T. Berlijn, W. Ku, B. M. Andersen, and P. J. Hirschfeld, Interpretation of Scanning Tunneling Quasiparticle Interference and Impurity States in Cuprates, Phys. Rev. Lett. **114**, 217002 (2015).

[42] P. Choubey, A. Kreisel, T. Berlijn, B. M. Andersen, and P. J. Hirschfeld, Universality of scanning tunneling microscopy in cuprate superconductors, Phys. Rev. B **96**, 174523 (2017).

[43] P. J. Hirschfeld, D. Altenfeld, I. Eremin, and I. I. Mazin, Robust determination of the superconducting gap sign structure via quasiparticle interference, Phys. Rev. B **92**, 184513 (2015).

[44] G. Blumberg, A. Koitzsch, A. Gozar, B. S. Dennis, C. A. Kendziora, P. Fournier, and R. L. Greene, Nonmonotonic $d_{x^2-y^2}$ Superconducting Order Parameter in $Nd_{2-x}Ce_xCuO_4$, Phys. Rev. Lett. **88**, 107002 (2002).

[45] H. Matsui, K. Terashima, T. Sato, T. Takahashi, M. Fujita, and K. Yamada, Direct Observation of a Nonmonotonic $d_{x^2-y^2}$-Wave Superconducting Gap in the Electron-Doped High-T_c Superconductor $Pr_{0.89}LaCe_{0.11}CuO_4$, Phys. Rev. Lett. **95**, 017003 (2005).

[46] J. Tersoff and D. R. Hamann, Theory of the scanning tunneling microscope, Phys. Rev. B **31**, 805 (1985).

[47] P. Choubey, W.-L. Tu, T.-K. Lee, and P. J. Hirschfeld, Incommensurate charge ordered states in the t-t'-J model, New J. Phys. **19**, 013028 (2017).

[48] P. Choubey, S. H. Joo, K. Fujita, Z. Du, S. D. Edkins, M. H. Hamidian, H. Eisaki, S. Uchida, A. P. Mackenzie, J. Lee, J. C. S. Davis, and P. J. Hirschfeld, Atomic-scale electronic structure of the cuprate pair density wave state coexisting with superconductivity, Proc. Natl. Acad. Sci. USA **117**, 14805 (2020).

[49] J. Böker, M. A. Sulangi, A. Akbari, J. C. S. Davis, P. J. Hirschfeld, and I. M. Eremin, Phase-sensitive determination of nodal d-wave order parameter in single-band and multiband superconductors, Phys. Rev. B **101**, 214505 (2020).

[50] S. Wang, P. Choubey, Y. X. Chong, W. Chen, W. Ren, H. Eisaki, S.-i. Uchida, P. J. Hirschfeld, and J. C. S. Davis, Scattering interference signature of a pair density wave state in the cuprate pseudogap phase, arXiv:2105.06518 [Nat. Commun. in press (2021)].

[51] A. Kreisel, R. Nelson, T. Berlijn, W. Ku, R. Aluru, S. Chi, H. Zhou, U. R. Singh, P. Wahl, R. Liang, W. N. Hardy, D. A. Bonn, P. J. Hirschfeld, and B. M. Andersen, Towards a quantitative description of tunneling conductance of superconductors: Application to LiFeAs, Phys. Rev. B **94**, 224518 (2016).

[52] S. Chi, R. Aluru, U. R. Singh, R. Liang, W. N. Hardy, D. A. Bonn, A. Kreisel, B. M. Andersen, R. Nelson, T. Berlijn, W. Ku, P. J. Hirschfeld, and P. Wahl, Impact of iron-site defects on superconductivity in LiFeAs, Phys. Rev. B **94**, 134515 (2016).